Materials Transactions, Vol. 65, No. 3 (2024) pp. 323 to 330

他誌発表論文　再録
一般財団法人 軽金属学会
Materials Transactions, Vol.65, No.3 (2024), pp.323-330

Oxidation/Carburization Behavior of TiC–Ti Composites and Improved Wear Resistance through Surface Modification

Ryo Tsukane[1], Kazuhiro Matsugi[2], Yong-Bum Choi[2] and Hiroyasu Tamai[1]

[1]*Tottori Institute of Industrial Technology, Tottori 689-3522, Japan*
[2]*Graduate School of Advanced Science and Engineering, Hiroshima University, Hiroshima 739-8527, Japan*

This study has developed a surface modified titanium carbide (TiC)–titanium (Ti) composite for application in dry press working. This material was synthesized through mechanical alloying using Ti and graphite powder, followed by spark plasma sintering, and subsequently surface-modified via oxidation/carburization treatment. The oxidation/carburization behavior was investigated to determine the treatment conditions that formed a hard coating layer, and its wear resistance was evaluated. The activation energy for the isothermal oxidation of this composite material was 271 kJ/mol, with the rate primarily determined by the O and Ti diffusion in titanium dioxide (TiO_2). In contrast, the activation energy for the growth of the carburized layer growth was 261 kJ/mol, with the rate determined by the carbon diffusion in TiC. The oxide film of the TiC–Ti composite material, oxidized by holding at 1073 K for 300 s, exhibited porous rutile TiO_2 with a thickness of approximately 1.7 µm and hardness of 11 GPa. The carburized layer of the TiC–Ti composite material, carburized at 1073 K and held for 2400 s, had a thickness of approximately 3 µm and hardness of 20 GPa. During a wear test utilizing a stainless-steel pin as the mating material, stainless steel adhered to the surface of the unmodified sample. The oxidized sample experienced wear due to the peeling of the oxide film. However, the carbonized sample neither adhered to nor wore the mating material, suggesting that the carbonization treatment helps to improve the wear characteristics. This study offers valuable insights into the fabrication of TiC-based cermets as mold materials for realizing dry press working.
[doi:10.2320/matertrans.MT-L2023014]

(Received September 21, 2023; Accepted December 4, 2023; Published February 25, 2024)

Keywords: *mechanical alloying, spark plasma sintering, cermet, TiC–Ti composite, thermal oxidation, carburization, wear resistance*

1. Introduction

The use of lubricants in plastic working, such as metal press working, is important for suppressing mold wear and seizure. However, this involves applying lubricants to work materials, cleaning, and removal after processing, which increases the task time and pollutes the work environment. In addition, most lubricants currently used in press working contain petroleum hydrocarbons, which generate carbon dioxide when incinerated, posing a burden on the global environment.[1] Consequently, dry press working, which avoids the use of lubricants, is increasingly sought after.

One possibility for realizing dry press working is via the utilization of ceramics as the mold material, as they demonstrate high hardness, low coefficient of friction (COF), and excellent wear resistance. Ceramic titanium carbide (TiC) has a high Vickers hardness of 3000 Hv and excellent adhesion resistance as a coating for plastic working dies.[2–4] However, the TiC coating peels off easily, with bulk TiC having poor toughness and being prone to defects, such as chipping, due to impacts experienced during processing. Therefore, the TiC toughness must be improved, which can be achieved effectively by combining it with metal materials.

Zhang *et al.* prepared nanostructured TiC particle-reinforced Ti-based composites *in situ* by mechanical alloying (MA) followed by spark plasma sintering (SPS) using Ti and graphite powders as reactants.[5] The toughness of this composite can be improved compared to that of monolithic TiC materials. However, as the composite contains a Ti phase that is susceptible to adhesion,[6] it may have poor tribological properties.

Two surface treatments were investigated to further improve the wear resistance of TiC–Ti composites, especially the wear resistance of the Ti phase in the surface layer. The first approach is the formation of TiO_2 by thermal oxidation, which was employed in previous studies to improve the frictional properties of Ti and its alloys.[7–9] The second approach is the formation of a TiC layer by carburization. Carburization treatment is an extensively used surface treatment method that primarily aims to improve the wear resistance of steel materials;[10–13] a similar effect has been reported for Ti materials.[14] However, these processes require adjusting the processing parameters to obtain optimal microstructures for the TiC–Ti composites.

In this study, the oxidation/carburization behavior was investigated to determine the treatment conditions required to form a hard coating layer. Subsequently, the effects of the surface modification of the TiC–Ti composites on their wear resistances were investigated.

2. Experimental

2.1 Fabrication procedure

Commercial Ti powder (<45 µm, oxygen concentration of 0.299 mass%, FUJIFILM Wako Pure Chemical Corp.) and graphite (C) powder (mean particle size of 5 µm, Kojundo Chemical Laboratory Co., Ltd.) were used in this study. The Ti and C powders with the C addition ratio of 28 mol% were mechanically alloyed in a planetary ball mill (Fritsch P-6). This ratio was based on the authors' previous work, where the effect of the C addition ratio on the properties of TiC–Ti composites was determined. At a C addition ratio of 28 mol%, the volume ratio between TiC (hard particle) and Ti (binder phase) was approximately 7:3, and a good balance of mechanical properties was obtained.[15] The materials and tungsten carbide balls (25 balls, φ10 mm) were added to an 80 mL tungsten carbide bowl in a glove box under an argon (Ar) atmosphere. The ball-to-powder mass ratio was 5.8:1, and the milling speed was 500 rpm for 10.8 ks.

The milled powder was loaded into a cylindrical graphite die (φ20 mm) with an interfacial graphite sheet coated with boron nitride to prevent reaction with the die. The powder was sintered by SPS (DR. SINTER SPS-3.20 MK-4, Sumitomo Coal Ming Co.) under vacuum at 1273 K, with a heating rate of 1.68 K/s, followed by a dwell time of 300 s at a uniaxial pressure of 35 MPa.

2.2 Thermal oxidation and carburization

Coupons of approximately $4 \times 4 \times 4\,mm^3$ were cut from the sintered samples, polished on a series of silicon carbide polishing papers up to #2000 (JIS), ultrasonically washed in an acetone bath, and dried in air to obtain information on oxidation and carburization kinetics. Isothermal oxidation studies were performed in air at temperatures of 873 and 1073 K for different durations. The oxidation behavior was evaluated by generating the mass-gain data as a function of time. The carburization treatment was examined using 99.7% pure C powder, with a mean particle size of 5 μm as the C source. A graphite container was filled with C powder, and a coupon cut out from the sintered sample was embedded in the C powder. Subsequently, the graphite container was exposed to Ar gas at 1073 and 1273 K for a specified time. The cross-section of the carburized coupon was emery-polished and buffed, and the thickness of the TiC layer on the surface was measured via scanning electron microscopy (SEM) which will be detailed below. The carburization behavior was evaluated by generating the TiC layer thickness-gain data as a function of time.

The microstructure of the composites before and after thermal oxidation and carburization was investigated by cross-sectional microscopy using field-emission gun SEM (FEG-SEM, SU5000, Hitachi High-Tech). The composition of the sintered samples was analyzed by SEM equipped with the energy-dispersive X-ray spectroscopy (EDS). The phase constituents were analyzed by X-ray diffraction (XRD, Ultima IV, Rigaku) using Cu-Kα radiation at 40 kV and 40 mA. The hardness was measured by a nanoindentation system (ENT-1100a, Elionix) using a Berkovich indenter. The maximum load was 10 mN, and the contact depth was maintained below 10% of the oxide film and carbonized layer thickness. The hardness, H, was calculated from the maximum load based on the Oliver and Pharr method:[16)]

$$H = P_{max}/A \tag{1}$$

where A is the projected area of the Berkovich indenter on the sample, and P_{max} is the maximum load used.

2.3 Wear tests

Sliding wear tests were performed using a pin-on-disk tribometer (TRIBOMETER, CSM Instruments). Dry sliding wear tests were performed on polished samples using a pin-on-disk configuration with a load of 5 N at a sliding speed of 0.2 m/s against a 3-mm-diameter stainless-steel (JIS SUS304) pin at 293–297 K. All sample surfaces were buffed to an average surface roughness (R_a) of 0.04–0.05 μm prior to testing. The R_a of the contact surface of the stainless-steel pin was set to 0.2 μm. The tests were conducted with a sliding distance of 100 m. After the test, the wear track properties were observed and measured by SEM and a stylus roughness tester (FORM TALYSURF PGI Plus, Taylor Hobson). The stainless-steel pins were ultrasonically cleaned prior to each test and weighted to $\pm 10^{-5}$ g using an electronic balance. After each test, the samples were cleaned to remove loose debris and weighed to determine the mass change.

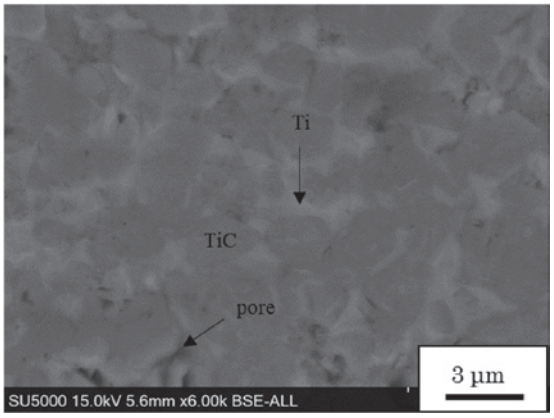

Fig. 1 SEM image of the microstructure of the TiC–Ti composite.

3. Results and Discussion

3.1 Characterization of the composites

The microstructure of the TiC–Ti composites comprised (1) a pore or C with a black component, (2) a Ti phase with a bright contrast, and (3) a TiC phase with a dark contrast, as shown in Fig. 1. The TiC phase was granular with Ti phases distributed in the gaps between the TiC grains. The analysis of the SEM images was used to determine ratios of 78, 20, and 2% for the TiC phase, Ti phase, and C or pore, respectively.

Figure 2 illustrates the backscattered electron composition image of the cross-section of a TiC–Ti composite subjected to oxidation/carburization treatment and the corresponding EDS map. The oxidized sample held at 1073 K for 300 s exhibits an oxide film of approximately 1.7 μm adhering to the substrate, as shown in Figs. 2(a) and (b). Figures 2(c) and (d) show a sample embedded in C powder and held at 1073 K for 2400 s. A large amount of C was distributed for approximately 3 μm on the surface layer, which is considered the carburized layer.

3.2 Oxidation and carburization kinetics

The kinetics of the isothermal oxidation (in terms of the mass gain per unit area as a function of time) for the TiC–Ti composite at 873 and 1073 K are presented in Fig. 3. The mass gain data in Fig. 3 indicate that the oxidation behavior obeys a parabolic rate law. In general, the isothermal-oxidation kinetic in the parabolic oxidation process is expressed by the power law as:[17)]

$$\Delta W = (k_p t)^{1/2} \tag{2}$$

where ΔW, t, and k_p are the mass gain per unit area, time, and rate constant, respectively. k_p follows an Arrhenius relation, as follows:

$$k_p^2 = k_0\, exp(-Q/RT) \tag{3}$$

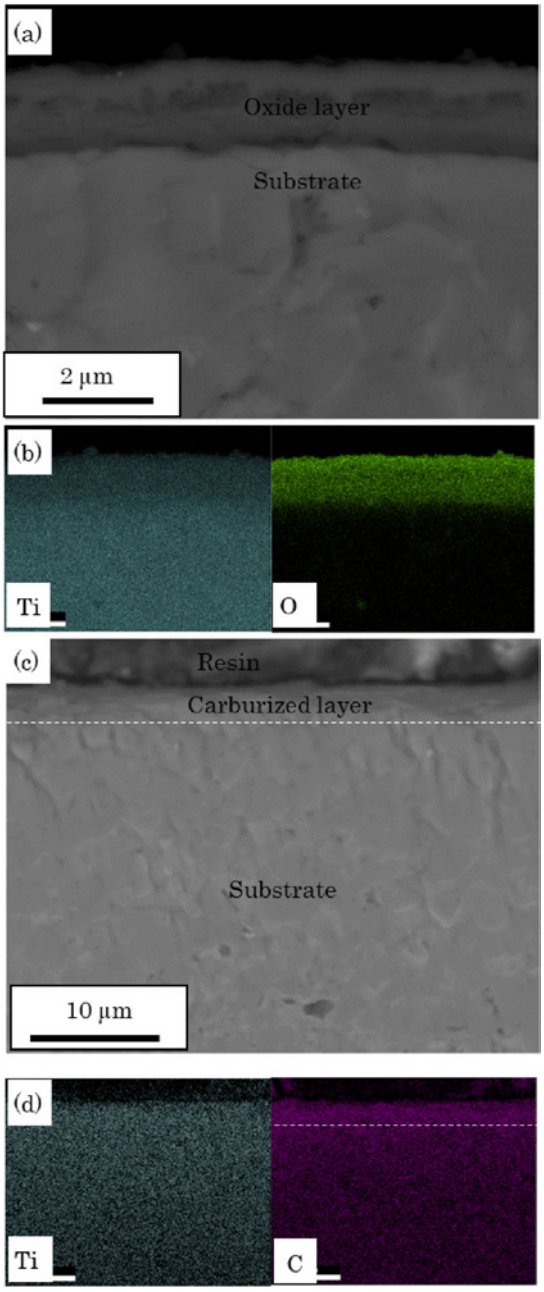

Fig. 2 Cross-sectional SEM images and corresponding elemental maps of the sample (a) and (b) oxidized at 1073 K for 300 s and (c) and (d) carburized at 1073 K for 2400 s.

where Q is the effective activation energy for oxidation, k_0 is the constant for a given material, T is the absolute temperature, and R is the gas constant.

Figure 4 depicts a plot of the square of k_p in a logarithmic scale versus $1/T$. The activation energy for the oxidation of the TiC–Ti composite, as observed from the slope of the plot, is 271 kJ/mol, which is higher than the activation energy for the oxidation of pure Ti (239 kJ/mol[18]). The activation energy for the oxygen (O) diffusion in α-Ti is 200 kJ/mol.[19] In addition, the activation energies for the O and Ti diffusion in TiO_2 are 234 and 250 kJ/mol, respectively.[18] Therefore, the activation energy for the oxidation of the TiC–Ti composites is similar to that for the O and Ti diffusion in

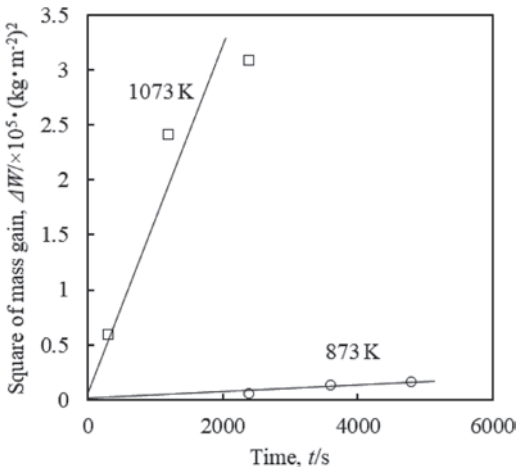

Fig. 3 Relationship between the square of the mass gain and time.

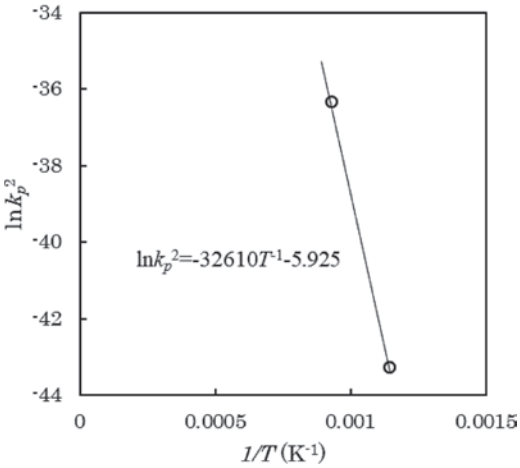

Fig. 4 Arrhenius plot of the parabolic rate constant (k_p^2) for the oxidation of TiC–Ti composites.

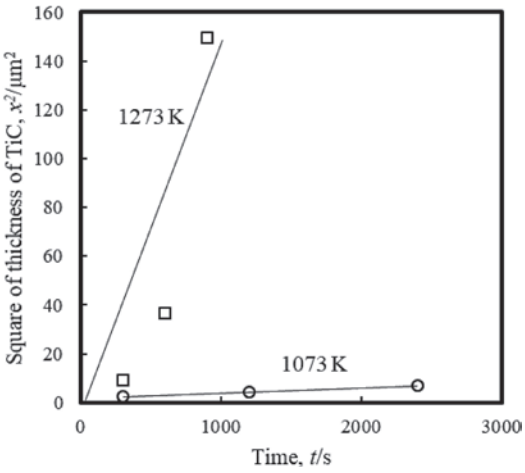

Fig. 5 Relationship between the square of the thickness of the TiC coating layer and time of the carburization treatment.

TiO_2, suggesting that this phenomenon is a rate-limiting process.

The relationship between the thickness of the carburized layer and holding temperature and holding time of the carburization treatment is shown in Fig. 5. The square of the

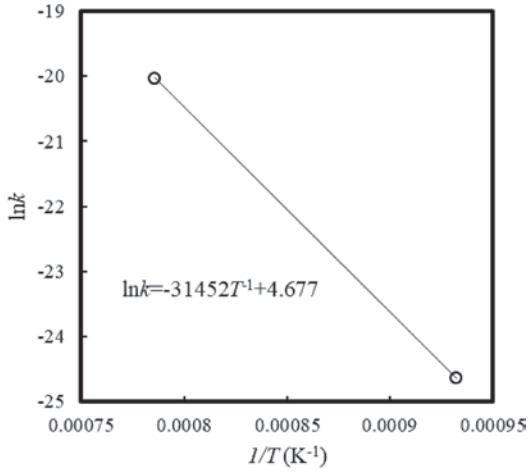

Fig. 6 Arrhenius plot of the parabolic rate constant (k) for the TiC growth in TiC–Ti composites.

carburized layer thickness increases linearly with the holding time. In other words, the growth of the carburized layer follows the parabolic velocity law given by the equation:

$$x^2 = kt \tag{4}$$

where x, t, and k are the carburized layer thickness, time, and rate constant, respectively. The rate constant k follows an Arrhenius relation, as follows:[20)]

$$k = k_0 \, exp(-Q/RT) \tag{5}$$

where Q is the activation energy of the carburized layer growth, k_0 is a constant, T is the absolute temperature, and R is the gas constant.

Figure 6 shows a logarithmic plot of k versus $1/T$. The activation energy for the carburized layer growth of the TiC–Ti composite is 261 KJ/mol. The activation energy for C diffusion in TiC is in the range of 236–460 kJ/mol.[21)] In comparison, the activation energy for the Ti diffusion in TiC is 740 kJ/mol.[21)] Therefore the activation energy for the growth of the carburized layer in TiC–Ti composites is similar to that for the C diffusion in TiC, suggesting that this phenomenon is a rate-limiting process.

3.3 Structure and properties of the oxidized or carburized layers

Figures 7(a) and (b) show the SEM images of the surface after buffing of an oxidized sample maintained at 1073 K for 300 s and a carburized sample maintained at 1073 K for 2400 s, respectively. The oxidized sample exhibits a porous structure, whereas the carburized sample surface is uniformly covered with TiC. The XRD results depicted in Fig. 8 confirm that the oxide film was rutile TiO_2.

The oxide layer of the TiC–Ti composite oxidized at 1073 K for 300 s covers the surface uniformly without cracking and/or spallation, as shown in Fig. 2(a), whereas that oxidized at 1073 K after 1200 s or more exhibits an oxide film separated in the middle. The Pilling–Bedworth ratio[22)] indicates the volume expansion rate associated with oxide formation, which is 1.78 for Ti and 1.55 for TiC. If the Pilling–Bedworth ratio is less than 1, the oxide film cannot cover the entire surface, and cracks appear in the film. In

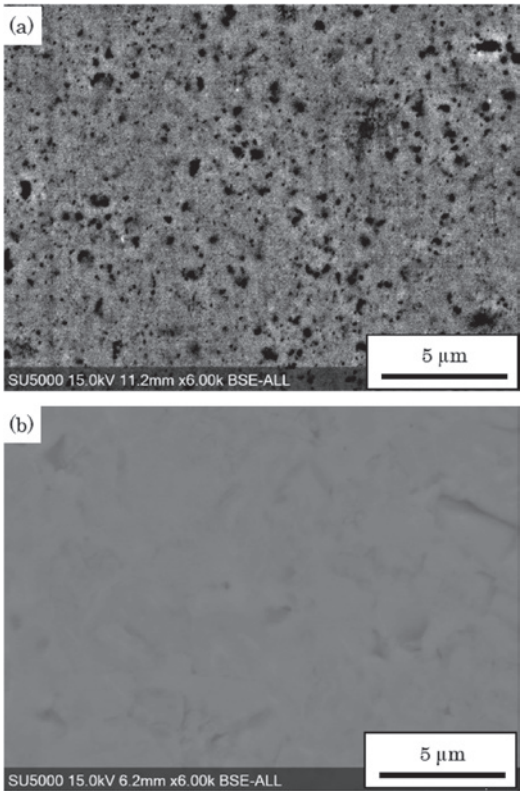

Fig. 7 SEM images of the surface after buffing the (a) oxidized sample held at 1073 K for 300 s and (b) carburized sample held at 1073 K for 2400 s.

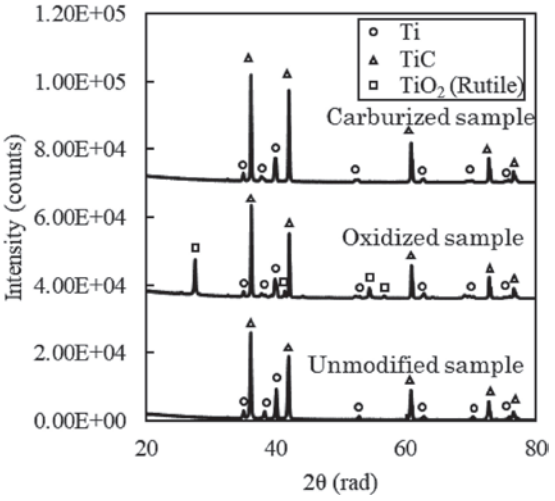

Fig. 8 XRD patterns of the unmodified, oxidized, and carburized samples.

contrast, when the Pilling–Bedworth ratio is greater than 1, as is the case in this study, a compressive stress is generated in the film. Therefore, the oxide film can cover the entire surface in the TiC–Ti composite material but a longer oxidation time may lead to a higher compressive stress in the film, causing the film to separate. As such, wear tests were performed on samples treated at 1073 K for 300 s.

When the carburization process was performed at 1073 K, Ra was approximately 0.09 μm, which improved to 0.048 μm by buffing. Meanwhile, the Ra of the sample after

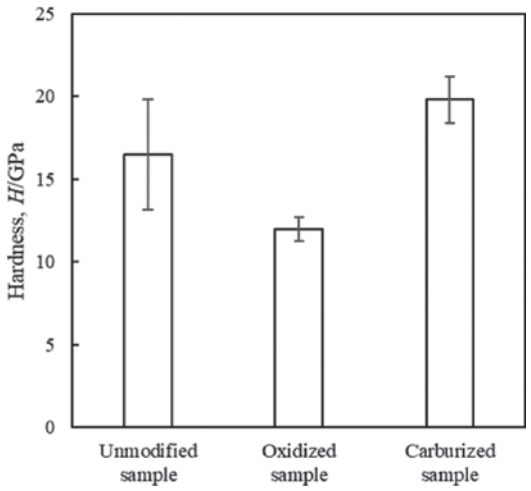

Fig. 9 Hardness of the sample surface.

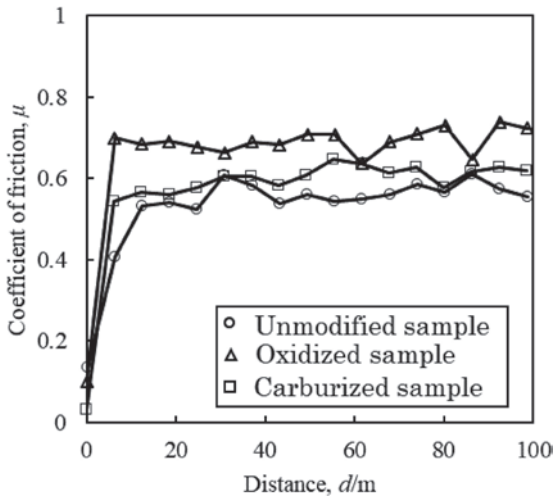

Fig. 10 Variations in the coefficients of friction as a function of the sliding distance of the samples.

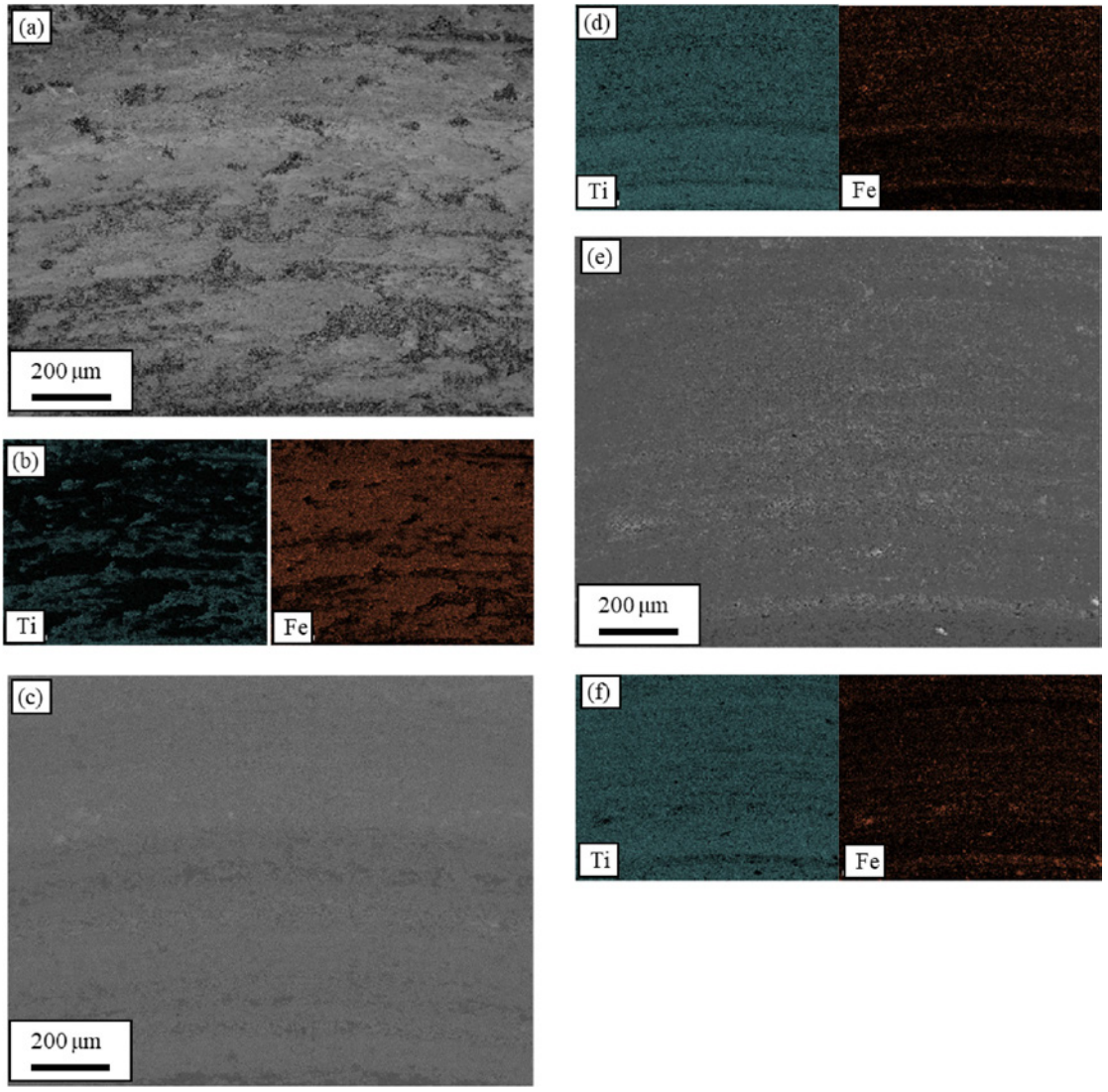

Fig. 11 SEM images and corresponding elemental maps of the disk wear tracks: (a) and (b) unmodified, (c) and (d) oxidized, and (e) and (f) carburized samples.

Table 1 Average compositions of the wear tracks of the disks, sliding surfaces of the pin, and debris analyzed by EDS.

	sample	mass%				
		Ti	Fe	O	Cr	Ni
disk	Unmodified sample	31.1	34.6	20.4	9.3	4.6
	Oxidized sample	58.3	6.8	32.1	1.8	0.9
	Carburized sample	64.5	7.9	24.1	2.4	1.1
pin	Unmodified sample	1.7	65.6	6.4	17.5	8.8
	Oxidized sample	2.6	62.6	9.7	16.6	8.4
	Carburized sample	1.1	64.1	9.0	17.2	8.6
debris	Unmodified sample	6.6	53.9	17.1	15.1	7.4
	Oxidized sample	36.4	9.9	49.4	2.9	1.4
	Carburized sample	3.5	39.0	42.8	9.5	5.2

carburization at 1273 K was 0.594 μm, which was not smoothed even by buffing. Therefore, wear tests were performed on samples carburized at 1073 K for 2400 s.

Figure 9 shows the surface indentation hardness results of the oxidized and carburized samples subjected to wear tests. The indentation hardness of the oxide layer was lower than that of the unmodified substrate, whereas the carburized layer exhibited the highest indentation hardness.

3.4 Wear tests

Figure 10 shows the evolution of the COF of the investigated samples. For all samples, the COF increased with the increase in the wear distance in the early stages of wear and then became almost constant. These constant values were almost equal for the unmodified and carburized samples, while those for the oxidized samples were slightly higher. In the wear track of the unmodified samples, Fe adhesion was confirmed (Fig. 11(a) and (b)). The wear tracks on the oxidized and carburized samples exhibit minimal transfer from the stainless-steel pin (Figs. 11(c), (d), (e) and (f)), as confirmed by the results of the quantitative EDS analysis (Table 1). Figure 12 shows the depth profiles of the wear tracks for each sample. The wear track of the unmodified sample exhibited no dents; instead, it was raised due to the adherence of deposits from the stainless-steel pin, forming a layer with a thickness of approximately 2 μm. In contrast, the oxidized sample exhibits wear on the surface with a wear track depth of approximately 2 μm. Notably, the surface of the carburized sample was neither convex nor concave and remained almost unchanged from the initial conditions.

Figure 13 shows the SEM image of the worn surface of the stainless-steel pin. The stainless-steel pin exhibits a significantly lower hardness value than that of all the materials used for the disk (approximately 1 GPa in indentation hardness). Moreover, continuous scratches were observed in the sliding direction on all wear surfaces, indicating abrasive wear as the main wear mode. The pin surface used for the unmodified sample (Fig. 13(a)) exhibited discontinuous wear scratches owing to partial detachment, which were not observed on the pin used as the oxidized/carburized sample (Fig. 13(b) and (c)). Based on the quantitative analysis results shown in Table 1, a little more

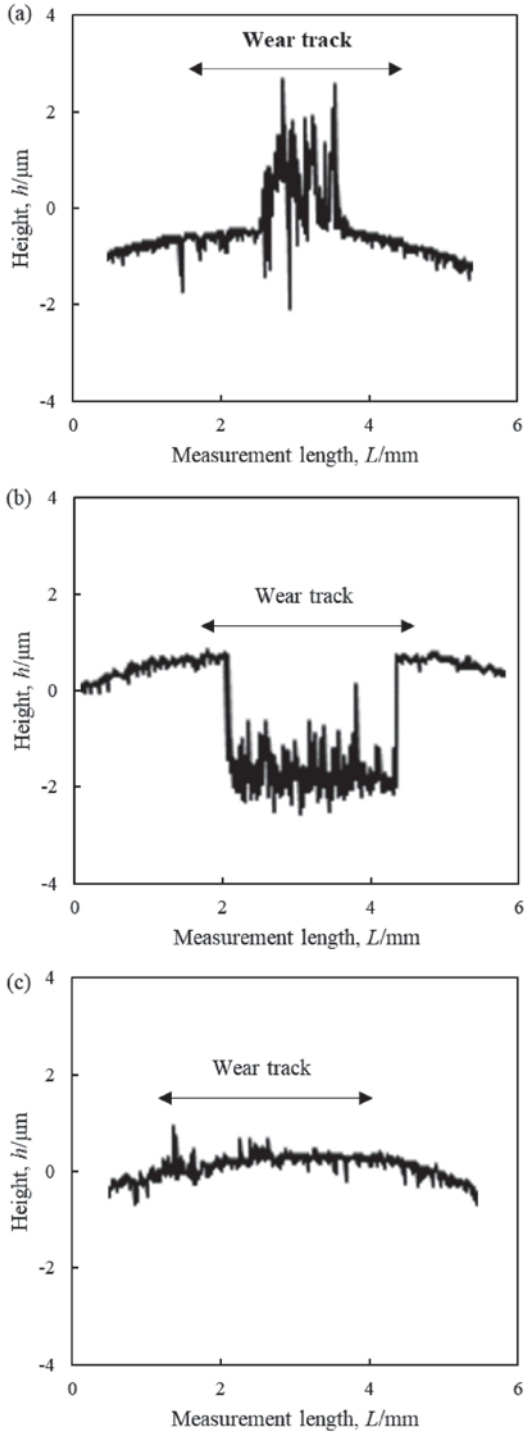

Fig. 12 Wear depth profiles of the wear track of the (a) unmodified, (b) oxidized, and (c) carburized samples.

Ti is present on the pin surface of the oxidized sample. The stainless-steel pin weight loss after the wear test was the highest for the pins used for the unmodified sample and the lowest for the oxidized sample, as shown in Fig. 14.

The wear mechanism of the TiC–Ti composite and stainless steel suggested by the above results is schematically shown in Fig. 15. First, the unmodified sample was considered, which is a disk with stainless steel adhering to its surface owing to the friction with the stainless-steel pin as

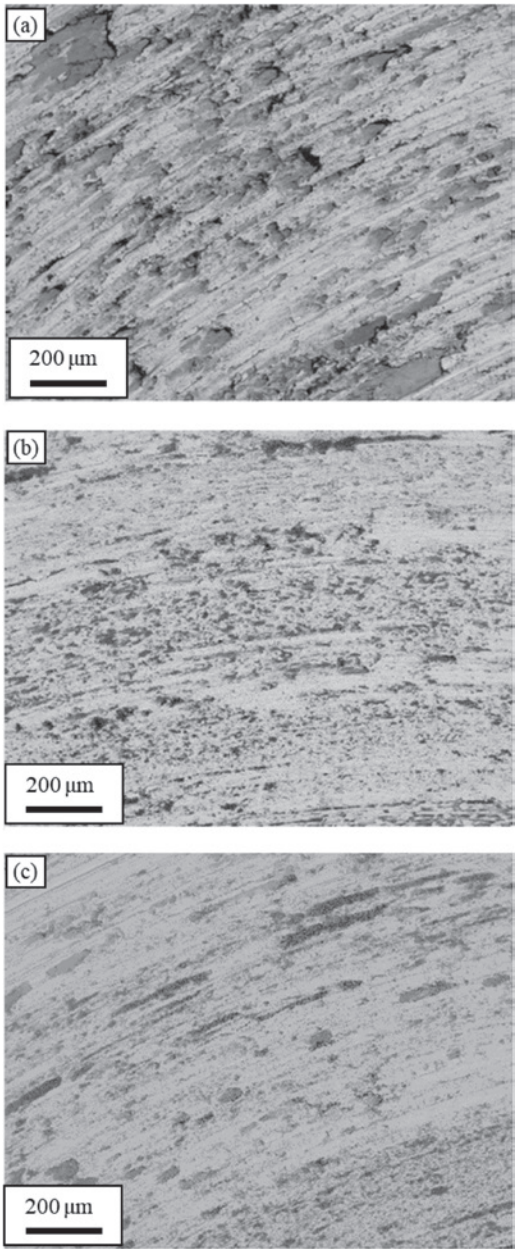

Fig. 13 SEM images of the sliding surfaces of the stainless-steel pin for the (a) unmodified, (b) oxidized, and (c) carburized samples.

the mating material. The hardness of the stainless-steel pin was significantly lower than that of the TiC–Ti composite surface, and abrasive wear occurred. Although the majority of the disk surface has a TiC phase, an active Ti phase accounts for approximately 20% of the surface area, whereby adhesion likely occurred. Notably, wear was not detected on the disk. The adhesion of Ti as the mating material was also observed on the stainless-steel pin. The wear powder had a metallic luster suggesting the occurrence of severe wear. Thus, the pin experienced both abrasive and adhesive wear.

As the TiO_2 rutile formed on the surface of the oxidized sample is chemically stable, adhesion of stainless steel did not occur. After the test, cracks were formed at the boundary between the oxide film and wear tracks, as shown in Fig. 16.

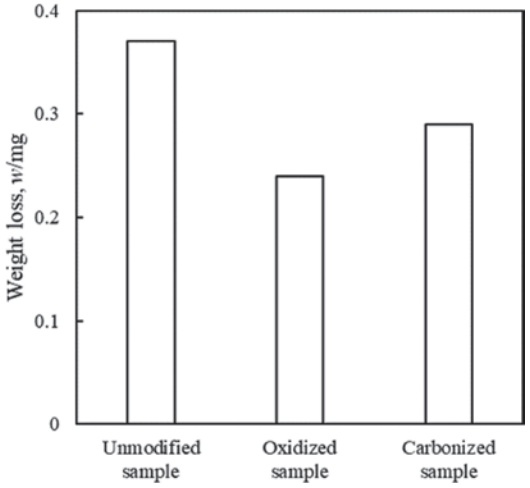

Fig. 14 Weight loss of the stainless-steel pin after the wear test.

The oxide film has a porous structure. Furthermore, since the TiO_2 rutile has a considerably different coefficient of the thermal expansion than Ti, stress is generated at the substrate/oxide film interface.[23] Therefore, cracks form in these voids, and the oxide film peels off. The hardness of the oxide film was the most similar to that of the stainless-steel pin among the three types tested. Therefore, the abrasive wear of the pin was considered less likely to occur.

As the TiC formed on the surface of the carburized product had excellent chemical stability, almost no adhesion occurred. Moreover, the highest indentation hardness for the carburized sample among the three sample denote that abrasive wear did not occur in the carburized disks but was observed in the pins. TiC has a thermal expansion coefficient similar to that of Ti, so stress is less likely to be generated at the substrate/carburized layer interface.[24] Therefore, it does not peel like an oxide film.

4. Conclusion

In this study, a TiC–Ti composite material synthesized by mechanical alloying using Ti and graphite powder, followed by SPS and subsequently surface-modified via oxidation/carburization treatment. The oxidation and carburization behavior was investigated to determine the treatment conditions that formed a hard coating layer, and its wear resistance was evaluated. The results obtained are summarized below.

(1) The activation energy for the isothermal oxidation of the composite material considered herein was 271 kJ/mol, and the rate was determined by the O and Ti diffusion in TiO_2. Further, the activation energy for the carburized layer growth was 261 kJ/mol, and the rate was determined by the C diffusion in TiC.

(2) The oxide film of the TiC–Ti composite material oxidized at 1073 K for 300 s was porous rutile TiO_2, with a thickness of approximately 1.7 μm and hardness of 11 GPa. The carburized layer of the TiC–Ti composite material carburized at 1073 K for 2400 s had a thickness of approximately 3 μm and hardness of 20 GPa.

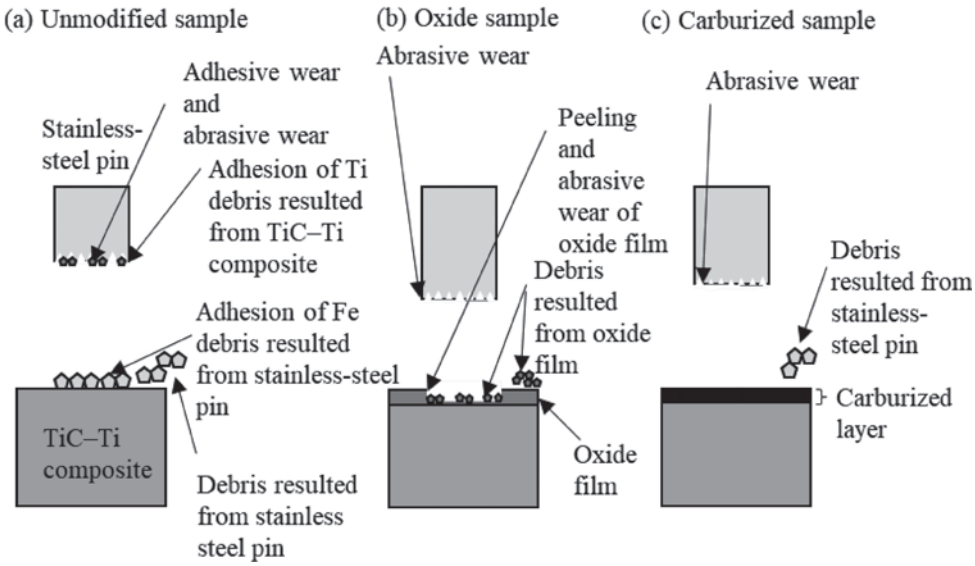

Fig. 15 Schematic of the wear mechanism of the TiC–Ti composite and surface-modified composites.

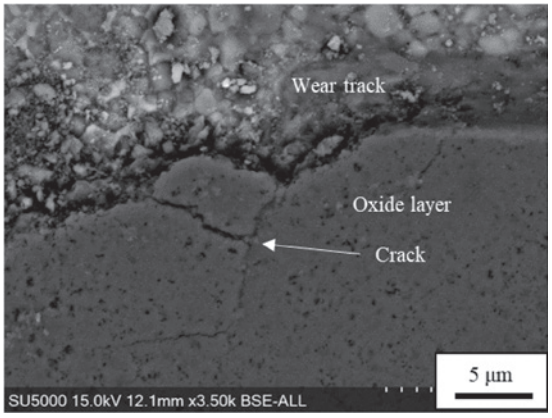

Fig. 16 SEM image of the cracks formed in the oxide film near the wear tracks.

(3) In the wear test using a stainless steel pin as the mating material, stainless steel adhered to the surface of the unmodified sample, while the oxidized sample was worn owing to the peeling of the oxide film. The carburized sample did not adhere to or wear the mating material, suggesting that carburization treatment contributes in improving the wear characteristics of the material.

Acknowledgments

This research was supported by the JKA public-interest-incorporated foundation. We gratefully acknowledge the subsidies from the bicycle and other machine industry promotion projects, which provided some of the equipment used in this study. The authors sincerely appreciate the financial support from the Amada Foundation. Special thanks go to Toshiyuki Ueno at Shimane Institute for Industrial Technology for his assistance with the SPS.

REFERENCES

1) S. Kataoka: J. JILM **55** (2005) 39–46.
2) A. Babapoor, M.S. Asl, Z. Ahmade and A.S. Namini: Ceram. Int. **44** (2018) 14541–14546.
3) A.S. Namini, Z. Ahmadi, A. Babapoor, M. Shokouhimehr and M.S. Asl: Ceram. Int. **45** (2019) 2153–2160.
4) K. Inoue, M. Suzuki, S. Nishino, Y. Tomota and K. Ohya: J. JSTP **52** (2011) 1073–1077.
5) X. Zhang, F. Song, Z. Wei, W. Yang and Z. Dai: Mater. Sci. Eng. A **705** (2017) 153–159.
6) J. Larson-Basse: National science foundation, introduction to friction, *ASM Handbook, Vol. 18, Friction, Lubrication and Wear Technology*, (ASM International, Metals Park, OH, 1992) pp. 27–28.
7) N. Dalili, A. Edrisy, K. Farokhzadeh, J. Li, J. Lo and A.R. Riahi: Wear **269** (2010) 590–601.
8) A.F. Yetim: Surf. Coat. Technol. **205** (2010) 1757–1763.
9) O. Çomaklı, T. Yetim and A. Çelik: Surf. Coat. Technol. **246** (2014) 34–39.
10) S. Takayasu, O. Umezawa and K. Hashimoto: Wear **502–503** (2022) 204397.
11) P. Zhang, F.C. Zhang, Z.G. Yan, T.S. Wang and L.H. Qian: Wear **271** (2011) 697–704.
12) B.M. Khusid, E.M. Khusid and B.B. Khina: Wear **165** (1993) 109–112.
13) M. Izciler and M. Tabur: Wear **260** (2006) 90–98.
14) T. Hayashi, K. Matsuura and M. Ohno: J. JILM **62** (2012) 233–236.
15) R. Tsukane, K. Matsugi, Y. Choi and H. Tamai: Book of abstracts of NERPS 2024 Conference in Hiroshima, Japan.
16) W.C. Oliver and G.M. Pharr: J. Mater. Res. **7** (1992) 1564–1583.
17) J. Dutta Majumdar, B.L. Mordike, S.K. Roy and I. Manna: Oxid. Met. **57** (2002) 473–498.
18) X.N. Zhang, C. Li, X.C. Li and L.J. He: Mater. Lett. **57** (2003) 3234–3238.
19) Z. Liu and G. Welsch: Metall. Trans. A **19** (1988) 1121–1125.
20) H. Sudo, I. Tamura and T. Nishizawa: *Kinzokusoshikigaku*, (Maruzen, Japan, Tokyo, 1972) p. 66.
21) B.B. Khina, B. Formanek and I. Solpan: Physica B **355** (2005) 14–31.
22) C. Xu and W. Gao: Mater. Res. Innov. **3** (2000) 231–235.
23) A. Moatti, R. Bayati and J. Narayan: Acta Mater. **103** (2016) 502–511.
24) T. Takahashi, K. Sugiyama and K. Tomita: Kinzoku Hyomen Gijutsu **18** (1967) 264–267.